Bulletin of the Mineral Research and Exploration

http://bulletin.mta.gov.tr

The importance of Confocal Raman Spectroscopy and mineral chemistry studies in the magma crystallization processes: Strandja Intrusives, NW Türkiye

Ezgi ULUSOY[a]* and Yusuf Kağan KADIOĞLU[b,c]

[a]General Directorate of Mineral Research and Exploration, Department of Geological Research, Ankara, Türkiye.
[b]Ankara University, Department of Geological Engineering, Ankara, Türkiye.
[c]Ankara University, Yerbilimleri Uygulama ve Araştırma Merkezi, Ankara, Türkiye.

ABSTRACT

The Strandja Massif cropping out in NW Turkey is cut by Late Cretaceous intrusives. These are called Strandja Intrusives and they are felsic and mafic coeval intrusives. Felsic intrusives consist of granite, granodiorite, quartz monzonite and syenite, while mafic intrusives consist of diorite and gabbro composition. Main composition of felsic intrusives consists of quartz, alkali feldspar, plagioclase, biotite, amphibole ±pyroxene mineral association, while main composition of mafic ones consists of plagioclase, biotite, amphibole ±pyroxene ±olivine mineral association. Amphiboles hydrated double-chain mineral of the Strandja Intrusives observed in all rocks used as an index mineral in this study to understand the petrological evolution of the rocks. According to Confocal Raman Spectroscopy studies amphiboles were actinolite type and exhibited similar spectrum and results of mineral chemistry reveals that they were calcic/Mg-hornblende types. According to geothermobarometer calculations, amphiboles crystallize in felsic intrusives at a pressure range of 0.49-0.94 kbar and a temperature of 757.52-814.49°C temperature at a depth of approximately 1.34-4.93 km, while in mafic ones at 2.59 kbar pressure and 892.82°C temperature at 9.97 km depth. Different temperatures-depth conditions and overlaps in Raman shift obtained from amphiboles indicate that these intrusives are derived from different sources but crystallized in the same environment.

1. Introduction

The scattering of the beam reflected on a component occurs in two ways: elastic (Rayleigh) and inelastic (Raman) scattering. If the light absorption event does not occur during the reflection of a violent monochromatic beam on any component, the light scattering event occurs, and this scattering is defined as Rayleigh scattering (Young, 1981; Skoog et al., 1998; Akçe and Kadıoğlu, 2020). The energy of a large part of the light scattered during elastic Rayleigh scattering is equal to the energy of the light interacting with matter (Table 1). In addition, the fact that a very small part of the reflected light is absorbed by the molecule, and the wavelength of the scattered beam is different from the wavelength of the reflected light, is defined as inelastic Raman scattering (Raman and Krishnan, 1928). While Rayleigh scattering gives a single peak with 104-105 times intensity compared to Raman scattering, it does not give any information about vibrational transitions of molecules. In addition, Raman scattering, which is the scattering of light

*Corresponding author: Ezgi ULUSOY, ezgi.ulusoy@mta.gov.tr

interacting with a molecule, provides information about the vibrational energy levels of molecules (Raman and Krishnan, 1928; Skoog et al., 1998; Akçe and Kadıoğlu, 2020; Karacan, 2020).

Table 1- Scattering types of light reflected on a material (Raman and Krishnan, 1928; Young, 1981).

Types of Scatterring the ray		
Scatter Type		**Situation**
Rayleigh	Elastic	Wavelength of scattered ray = Wavelength of the incident ray
Raman	Inelastic	Wavelength of scattered ray > Wavelength of the incident ray Wavelength of scattered ray < Wavelength of the incident ray

Raman scattering is the basis of Confocal Raman Spectrometry (CRS) research. In Raman scattering, there is a difference between the wavelength of the beam reflected on a solid-liquid-gas molecule and the wavelength of the reflected rays back. Decoupled raman scattering is a reflection of a solid-liquid-gas molecule. These differences are defined as Raman shift and contain important information about the chemical structure of the molecule (McMillan and Hofmeister, 1988; Ferraro et al., 2003). Raman studies of liquid and solid phases can be identified with the individual, the degree of crystallinity can be estimated with the result that many more of the data obtained can be used as a representative for temperature and density, and the abundance of each liquid component can be estimated, based on the characteristic of the Raman spectrum and in addition the ability to determine the molecular structure of a sample can be estimated due to polymerization (Bodnar and Frezzotti, 2020). Confocal Raman spectroscopy is a mineral that is sent with the wavelength of light emitted Raman shifts after the interaction with the molecule are called differences in the wavelength of light, and these spectra, which can reflect the identity of the mineral (Chukanov and Vigasina, 2020). The main vibration zones in the Raman spectrum according to mineral groups are generally shown in Figure 1. In addition, CRS studies show that minerals with a special solid solution (Ca-Mg carbonates, olivines, pyroxenes and tourmalines, etc.) also provides information about their chemical composition (Watenphul et al., 2016). Therefore, CRS analyses also provide useful data on qualitative phase identification and/or quantitative phase characteristics in mineralogical, crystallographic, geochemical, gemological and related sub-branches in the earth sciences (Nasdala and Schmidt, 2020; Ferrando, 2018).
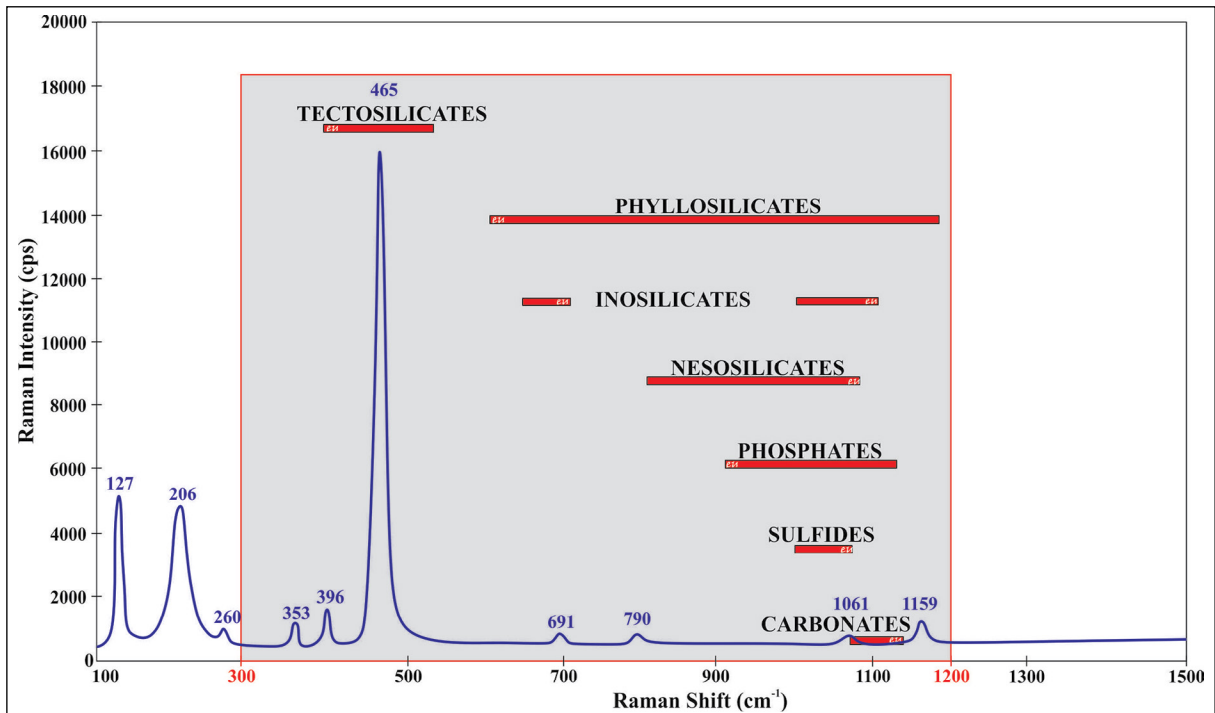

Figure 1- The main vibration zones of the most commonly observed mineral groups (Frezzotti et al., 2012; Ferrando, 2018).

Various approaches can be made about the crystallization processes of magma by performing CRS applications on the mineral components contained in intrusive rocks (Zoroğlu and Kadıoğlu, 2007; Deniz, 2010; Kadıoğlu et al., 2019; Akçe and Kadıoğlu, 2020; Ulusoy, 2021; Deniz, 2022). The differences in the Raman spectra obtained vary depending on the chemical structure of the molecules and thus minerals of different composition can be identified by distinguishing them according to their distribution and behavior in the Raman spectrum. For example, the fact that the mineral formed by elements/ions such as Na, Ca, Mg, Al and OH belonging to the amphibole group gives a different spectrum depending on the molecular structure may be due to the compositional difference of the amphibole mineral, and the size and uniformity in the spectrum may be due to the physical behavior and chemical purity of the amphibole mineral. In this way, it will be possible to distinguish the composition, type and different physical characteristics of the mineral that it has acquired during the crystallization period and/or later with the shift peaks in the Raman spectrum shown by the minerals.

Studies on the petrology and formation conditions of intrusive rocks outcropping in Anatolia, continue to be developed and updated, as well as useful studies conducted until today (Aydın et al., 2019; Kuşçu et al., 2019; Deniz and Kadıoğlu, 2019; Aydınçakır et al., 2020; Özdamar et al., 2021; Deniz, 2022). As first time in this study; By determining the changes in the crystallization processes of magma and the compositional behaviors of each rock group in the crystallization differentiation process by using the changes in the CRS spectra and the mineral chemistry data of the mafic mineral (amphibole) content common to all rock groups belonging to the Late Cretaceous Strandja Intrusions outcropped in NW Turkey, it is aimed to elucidate the petrological evolution of the region.

2. Geology of the Study Area

Turkey, located in the Alpine Himalayan Mountain Belt, consists of the amalgamation of many microcontinents and associations (Şengör and Yılmaz, 1981; Okay and Tüysüz, 1999). The rock units belonging to the Strandja Massif are outcropped from NW Turkey and expanding towards Bulgaria. The Strandja Massif is covered in the south by Tertiary sediments belonging to the Thracian Basin, while in the west it is cut by the strike-slip, N-S trending Western Black Sea fault (Okay et al., 2001) (Figure 2). The basement rocks of the Strandja Massif consist of pre-Permian aged crystalline rocks that lately metamorphosed and Late Variscan intrusions that cut the metamorphic basement (Aydın, 1982; Sunal et al., 2006; Okay et al., 2008; Natal'in et al., 2016). All the basement units underwent metamorphism and deformation under the conditions of the greenschist-amphibolite facies during the Variscan orogeny (Okay and Yurtsever, 2006). The bassement units are overlain by Triassic-Jurassic sedimentary cover units, that changes from clastic to carbonated, were metamorphosed under the lower amphibolite-upper greenschist conditions (Aydın, 1974, 1982; Chatalov, 1988; Okay et al., 2001; Okay and Yurtsever, 2006; Natal'in et al., 2005; Bedi et al., 2022), these units finally underwent regional metamorphism and compressional deformation during the Late Jurassic (Aydın, 1988). During the Alpine Orogeny, the Late Cretaceous aged intrusions are cut the Massif as a result of the closure of the Neotethys Ocean (Figure 3) (Aydın, 1974, 1982, 1988; Aykol, 1979; Moore et al., 1980; Ohta et al., 1988; Üşümezsoy, 1990; Aykol and Tokel, 1991; Çağlayan and Yurtsever, 1998; Karacık and Tüysüz, 2010; Ulusoy, 2012; Ulusoy, 2021; Ulusoy and Kadıoğlu, 2021; Bedi et al., 2022). According to geochemical data, these intrusions have a subduction-related origin (Aykol and Tokel, 1991; Karacık and Tüysüz, 2010). Biotite-hornblende-whole rock K-Ar and Ar-Ar ages indicate that the age of intrusions are in the Santonian-Campanian range (Moore et al., 1980; Ohta et al., 1988; Kuşçu et al., 2019; Ulusoy, 2021). All units belonging to the massif are unconformably covered by Upper Cretaceous sedimentary, volcano-sedimentary and volcanic units that are not metamorphosed (Aydın, 1982; Okay and Yurtsever, 2006). These volcanics belonging to the volcanic-plutonic complex in the Eastern Srednogorie zone are the product of the same system and are associated with Late Cretaceous aged intrusions (Okay and Yurtsever, 2006).

3. Analytical Methods

Strandja Intrusions are divided into two main groups as felsic and mafic intrusive rocks according
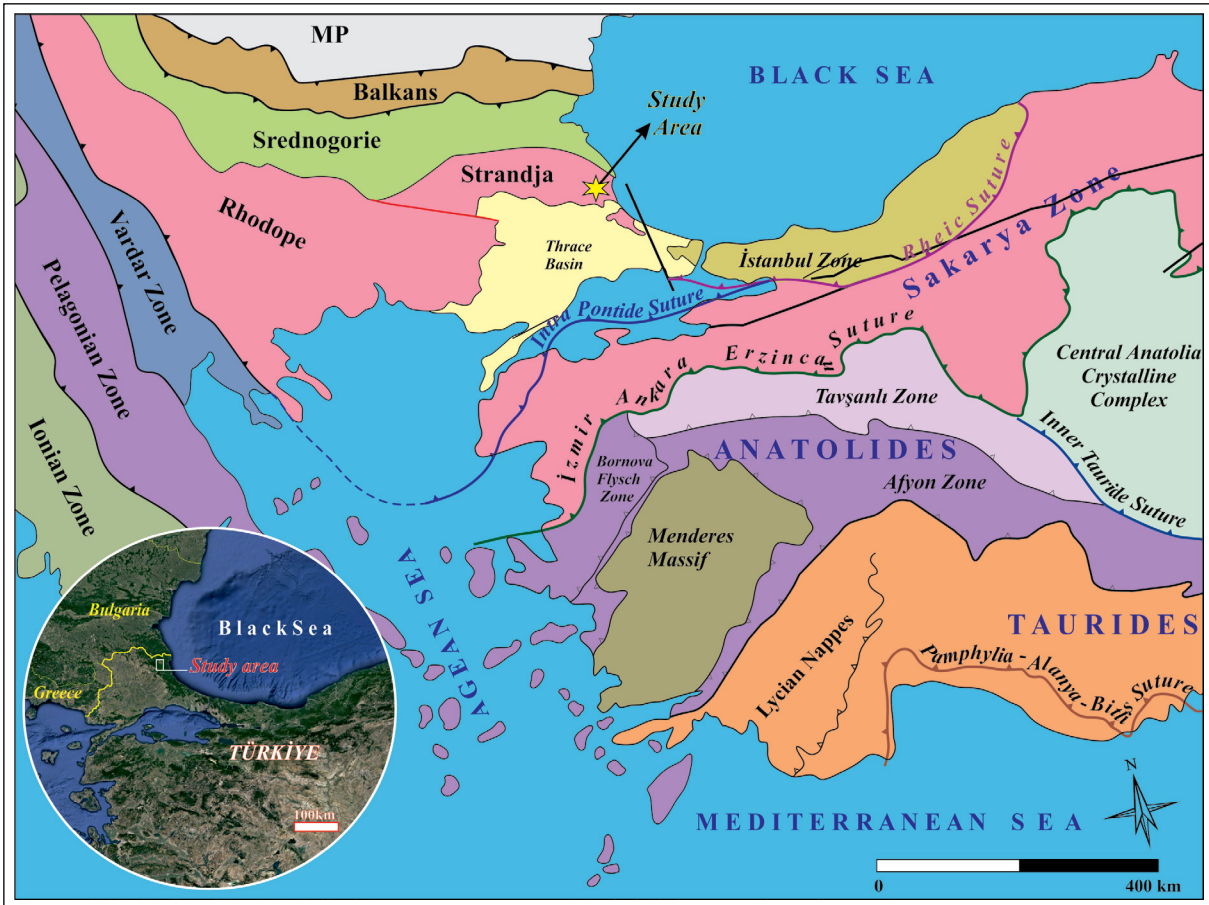
Figure 2- Location of the study area within the tectonic units of Türkiye (MP: Moezya Platform) (Map is modified from Okay and Tüysüz, 1999; Catto et al., 2018; and Candan et al., 2016).

to their compositional differences (Ulusoy, 2021). Detailed textural and mineralogical investigation of the representative samples selected from the rocks belonging to these groups were performed under a polarizing microscope and instrumental analyzes were performed.

Semi-qualitative CRS analyses and quantitative electron probe microanalysis (EPMA) of amphibole minerals from samples representing each rock group belong to the Strandja Intrusions were performed at the Ankara University Geosciences Application and Research Center. CRS examinations were performed with Thermo brand DXR model CRS device. The main components of the CRS measurement system consist of a laser, an electrically cooled charge-coupled device detector (CCD), an optical microscope. The device calibration was tested using polystyrene film.

Raman spectra with a resolution of 2 cm^{-1} in the range of 0-1200 cm^{-1} were obtained by using 633 cm^{-1} laser from the open thin sections of the samples. Mineral identification was made according to the spectra. After the polished sections of the same rocks were coated with carbon with Qurorum Q150TES device, the selected crystals were analyzed with JEOL brand JXA 8230 model Super Probe equipped with five wavelength dispersive spectrometer with a current of 20 kV and an acceleration voltage of 20 nA. Natural oxide and mineral reference materials were used for calibration and measurements. The conditions of the sample preparation and analysis process were carried out as defined in Deniz (2022). In the obtained data, matrix effects were corrected with the software provided by JEOL and corrections were made for atomic number (Z), absorption (A) and fluorescence (F) effects.
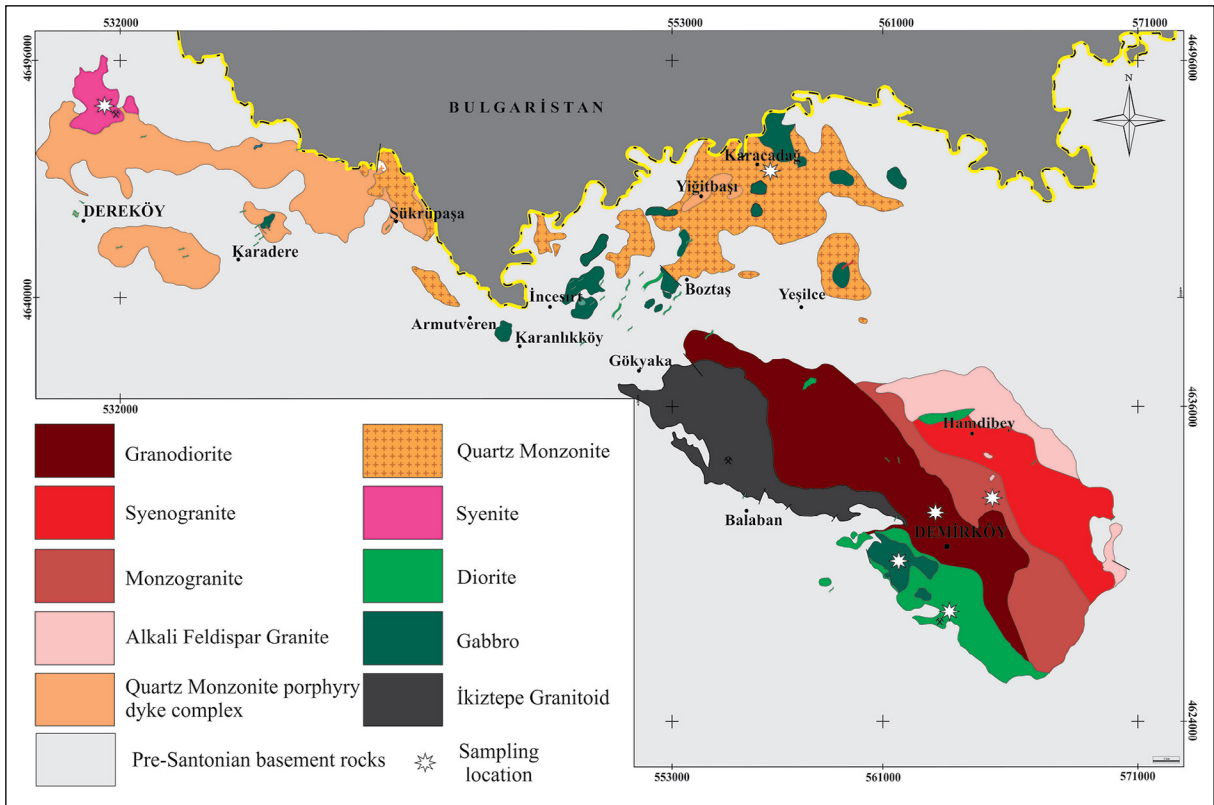
Figure 3- Compositional and positional distribution map of Late Cretaceous aged Strandja Intrusions outcropped in the study area (Ulusoy, 2021).

4. Results

4.1. Mineralogy - Petrography

The Late Cretaceous aged Strandja Intrusions that cut through the Strandja Massif are divided into two main groups as felsic and mafic. Macroscopically, the rocks are generally observed to be coarse-grained, phaneritic textured; microscopically, they exhibit holocrystalline hypidiomorph granular texture (Figure 4). The felsic intrusions are composed of granite, granodiorite, quartz monzonite and syenite. The main mineral content of the felsic group is quartz +plagioclase (oligoclase-andesine) +orthoclase in varying proportions depending on its composition. Varying amounts of biotite +amphibole in granites and granodiorites; in addition to these minerals,

	1 Granite	2 Granodiorite	3 Quartz Monzonite	4 Syenite	5 Diorite	6 Gabbro
Texture	Holocrystalline hypidiomorphic	Holocrystalline hypidiomorphic	Holocrystalline hypidiomorphic	Holocrystalline hypidiomorphic	Holocrystalline hypidiomorphic	Holocrystalline hypidiomorphic
Main minerals	KF, Q, PLG	PLG, Q, KF	PLG, KF, Q	KF, PLG, Q	PLG ± Q ±KF	PLG ± Q ±KF
Mafic minerals	Biotite, amphibole	Biotite, amphibole	Biotite, amphibole, clinopyroxene	Biotite, amphibole, clinopyroxene	Biotite, amphibole, clinopyroxene	± Biotite, amphibole, clinopyroxene ± olivine
Accessory minerals	Titanite, rutile, apatite, zircon, opaque min.	Titanite, rutile, apatite, zircon, opaque min.	Titanite, rutile, apatite, zircon, opaque min.	Titanite, rutile, apatite, zircon, opaque min.	opaque min.	opaque min.

Figure 4- Summary of petrographic characteristics of rock groups belonging to Strandja intrusions (AF: alkali feldspar, K: quartz: Plj: plagioclase, red highlighted mineral represents the mafic phase common to all rock groups).

clinopyroxene constitutes the mafic mineral composition in quartz monzonite and syenite. In addition, the syenite in the study area, unlike monzonite, contains less nepheline, which is another distinguishing feature. Some fine-grained titanite, allanite, apatite, zircon crystals and scattered magnetite crystals are located secondary to the rock groups. Mafic intrusions are composed of diorite and gabbro and cut felsic intrusions. In the field observations, dioritic compositional rocks have been evaluated in mafic intrusions due to their gradual transition with gabbro. The main composition of mafic rocks is plagioclase, amphibole, clinopyroxene ±biotite ±olivine ±orthoclase ±quartz. Magnetite, ilmenite and pyrite are scattered in varying proportions in mafic intrusions. In the studied rocks belonging to Strandja Intrusions, zoning in plagioclases and partially in coarse-grained minerals (orthoclase, plagioclase, amphibole, etc.), while poikilitic texture is observed. The coexistence of poikilitic and zoned texture indicate that crystallization may have continued in an irregular temperature range. Kaolinization and sossuritization in feldspars; magmatic uralitization observed in some of the clinopyroxenes and defined by the transformation only to amphibole group minerals from the crystal rim,

as well as epidotization and chloritization observed in some parts of mafic components.

4.2. Confocal Raman Spectroscopy

Within the scope of this study, CRS investigations of mafic component amphiboles, which are found in varying proportions in all rock groups constituting the felsic and mafic components of the Strandja Intrusions, were carried out. During the investigations, care was taken to select the amphibole crystals from euhedral and/or subhedral amphibole crystals that do not decompose as much as possible. The distribution of numerical values of characteristic Raman shifts of amphibole minerals crystallized in Strandja intrusions according to spectral regions is given in Table 2.

Ranges in the amphibole spectrum; the region of vibrations from the interactions between the cation and oxygen (M-O), internal Si_4O_{11} consists of band vibrations and OH molecule vibrations (Apopei and Buzgar, 2010). Raman shift spectrum of amphibole is $625 cm^{-1}$ the underlying spectral fields consist of the bending (deformation) field of the double chain silicate and vibrations in various M regions containing cations (Kloprogge et al., 2001; Rinaudo et al., 2004;

Table 2- Characteristic Raman shift values of amphibole minerals crystallized in the Strandja Massif.

	Spectral Region	Si-O-Si	O-Si-O	Si-O-Si	Si	SiO$_4$O$_{11}$-OH	T-M- OH (M: Mg,Fe)
	Raman Shift (cm^{-1})	*1200-1021*	*1021-735*	*735-500*	*500-383*	*383-173*	*173-50*
Rock Types	Gabbro	•1020.27	•818.36	•661.43	•535.12	•366.70 •319.34	•155.22
	Diorite			•667.17	•526.50	•383.93 •358.09 •218.38	•173.41 •152.35
	Syenite	•1021.16	•922.72 •735.74	•665.78 •564.86 •524.00	•406.99 •383.46	•359.93 •291.21 •216.91	•171.10 •150.05 •134.57 •112.28
	Quartz Monzonite	•1049.02		•728.93 •665.78 •561.15 •526.48	•408.84 •385.93	•363.65 •292.45 •217.53 •173.57	•151.90 •115.38
	Granodiorite		•1014.35 •917.15	•728.31 •663.92 •527.72	•383.46	•362.41 •289.97 •217.53 •174.19	•153.14
	Granite	•1045.31	•927.67	•668.88 •528.33	•388.41	•366.12 •220.63 •176.67	•155.00

Petry et al., 2006). 300-420cm^{-1} spectral region between T (M-OH), 420-610 cm^{-1} the spectral region is composed of Si-O-Si bending vibrations (Makreski et al., 2006). T denotes the transition mode and M denotes the Ca-Fe-Mg cations. 625-1130cm^{-1} the spectral region is caused by the internal vibrations of the crystal and consists of symmetrical (Vs) and asymmetric (Vas) vibrations of the Si-O-Si and O-Si-O bonds that make up the crystal (Kloprogge et al., 2001; Rinaudo et al., 2004).

As a result of CRS investigation of amphiboles contained in rocks of different compositions in the study area, it was determined that the amphiboles are in the composition of actinolite. When the spectra of actinolite amphiboles detected in the samples are examined, it is observed that the spectra overlap with each other in general (Figure 5). When the raman shifts of Mg-hornblend and Na-amphibole (riebeckite) are compared with the Raman shifts of the Strandja Intrusion amphiboles, it is observed that the amphiboles of the Strandja Intrusions differ significantly from the Na-amphibole (riebeckite) reference member, while they clearly show similarity to the Mg-Hornblend reference member. Raman shift peaks observed between 420-10 cm^{-1}, expressing OH release and lattice transition, show a change from felsic intrusives to mafic intrusives. The peaks of OH release and lattice transition show low amplitude in the early phase of magmatism and increase in later phases (Kadıoğlu et al., 2019; Güllü et al., 2019). Amphiboles representing the high temperature mineral in granites give relatively low amplitude peaks, while amphiboles in gabbros give higher amplitude peaks due to relatively being a lower temperature mineral. Güllü et al. (2019) stated that the Si4O11 bending mode OH bond amplitudes of amphiboles crystallized in the late phase are higher in amphibole minerals crystallized in the early phase.

Similarly, the high amplitude OH bond developed in such amphiboles in the Strandja Intrusives may also be related to the H2O concentration in the late stage residual magma. In this context, the rock groups evaluated as early stage in the study area represent rocks with gabbro-diorite composition, while the late stage rock groups are represented by granite and granodiorites.

In addition, the presence of magma mixing processes in intrusive rocks that outcropped in the study area can be supported by the similarity of the raman spectra of amphibole contained in granite and amphibole contained in gabbro-composed rock. Amphiboles are determined as hornblende under the optical microscope and mineral chemistry analyzes as actinolites in CRS investigation can similarly be explained by magma mixing processes. It is observed that the composition of the intrusions in the study area varies from mafic to intermediate and felsic composition. According to the geological, petrographic and spectroscopic data obtained, magma mixing is observed in all rocks (Ulusoy and Kadıoğlu, 2021; Ulusoy, 2021). In this context, it is observed that a certain part of the amphiboles exhibits changes from actinolite to chermachite as a result of magmatic uralitization. In mafic minerals crystallizing from the source magma of gabroic rocks, OH bonding cannot be expected under normal conditions, but crystallization of hydrous silicates (amphibole group minerals) can occur by mixing with felsic magmas during the crystallization periods of such magmas and interacting acidic and mafic elements.

When the Raman shift spectra of all amphiboles were compared, it was determined that they were distributed in 6 separate bands (Figure 5). It was determined that the Raman shift spectra of all the rocks in the group showed significant overlap and showed a broader spectrum range, especially by expanding in the SiO_4O_{11}-OH release band from gabbro to granite. The liberalization of the spectrum in the OH band can be explained by the increase in the water content of magma from gabbro to granite and, as a result, the crystallization of hydrous mafic (actinolite) silicates (Figure 5 and Table 2).

4.3. Chemistry of Amphiboles

Amphiboles, which are hydrous, double chain silicate minerals, are the most common mafic mineral among all rock groups in the study area. Amphibole minerals of varying crystal size are semi-octagonal and octagonal in shape, and partially coarse-grained crystals exhibit poikilitic texture. In general, amphiboles in rocks belonging to Strandja Intrusions display a homogeneous structure under microscope. Serial point measurements were made from amphibole
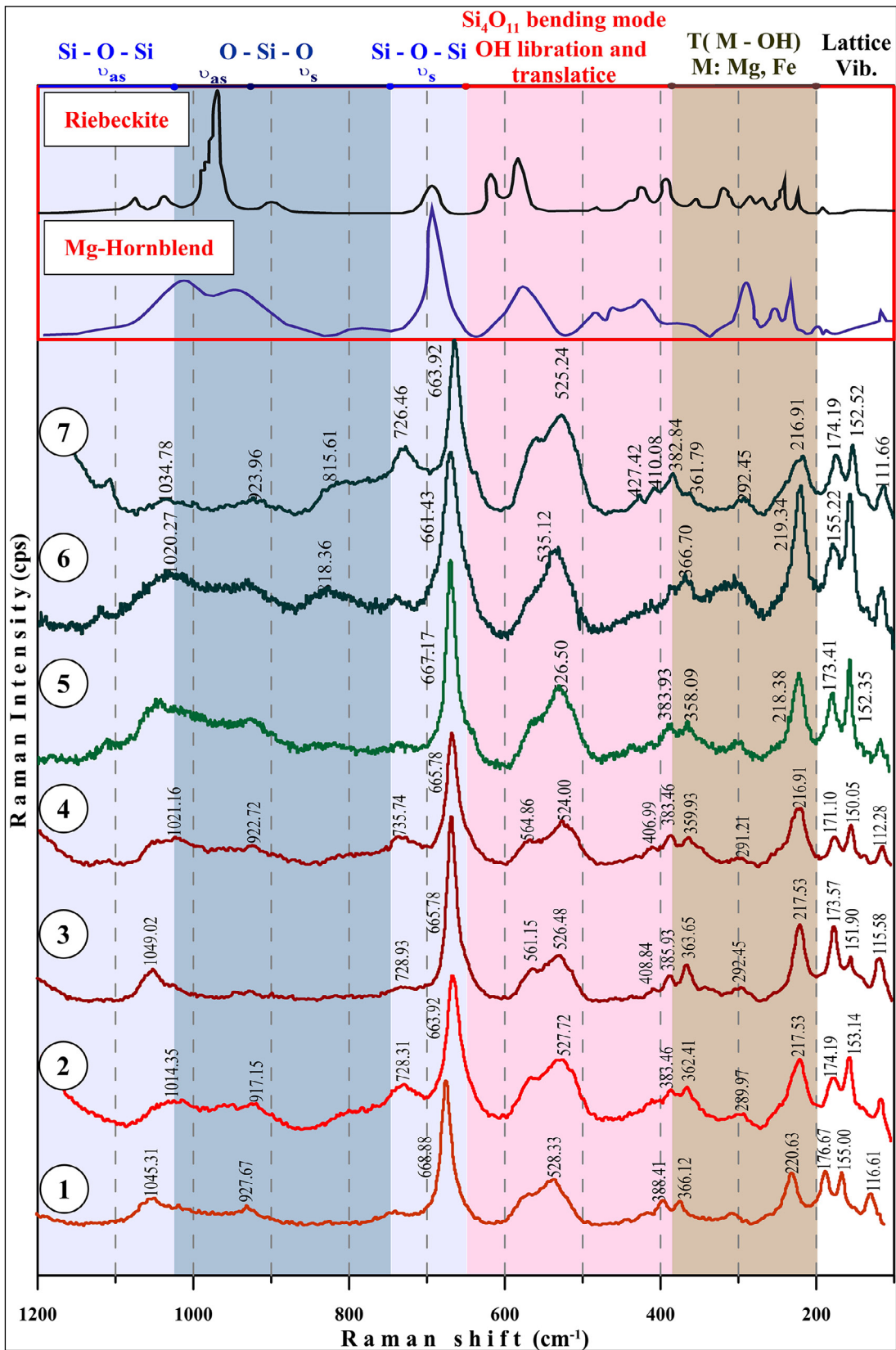
Figure 5- Comparison of the Raman spectra of amphibole crystals selected from each rock group with the Raman shift peaks of sodic and calcic amphibole minerals taken as reference (*: RRUFF, 2021; Ruff.info Riebeckite taken from the site and MG-Hornblende reference peaks) (1: Granite (Monzogranite), 2: Granodiorite, 3: Monzonite Quartz, 4: Syenite, 5: Diorite, 6: Gabbro).

crystals selected from felsic and mafic rock groups along a line from the rim to the core.

According to the obtained anoxide values, stoichiometric calculations were performed and the number of cations contained in each point was determined. The cation numbers and mineral structure were calculated according to Leake (1997) by taking 23 O. The representative mineral chemistry of the amphiboles belonging to the rock groups examined, the anoxide values and the calculated cation values as a result of the analysis are given in Table 3.

In the Al^{vi} versus Al^{vi} variation diagram, all amphiboles fall into the unaltered calcic magmatic amphibole fields (Figure 6a). According to the distribution of the points where the (Ca + Na) B values are greater than 1 on the BCa + BNa versus BNa exchange diagram, all of the samples have a calcic composition (Figure 6b). In the distribution of points where CaB is greater than 1.50 and (Na+K)A and CaA values are less than 0.50 in the $Mg/(Mg+Fe^{+2})$ versus Si exchange diagram, it is observed that most of the amphiboles fall into the Mg-hornblende area, and a small number of points is located at the border of actinolite and chermakite (Figure 6c). The distribution

Table 3- Representative mineral chemistry analysis results of the samples belonging to the studied rock groups.

| Sample	Granite			Granodiorite			Quartz Monzonite			Syenite			Gabbro		
	1	*2*	*3*	*1*	*2*	*3*	*1*	*2*	*3*	*1*	*2*	*3*	*1*	*2*	*3*
SiO_2	48.30	49.71	50.97	47.84	46.11	49.38	50.64	51.18	50.23	51.51	51.23	49.49	43.68	50.58	43.41
TiO_2	0.84	0.69	0.55	0.64	1.75	0.57	0.69	0.84	0.94	0.45	0.56	1.06	2.14	0.20	2.18
Al_2O_3	6.36	4.97	4.50	5.91	8.13	5.11	4.05	3.86	4.23	3.27	3.41	4.85	10.33	4.62	11.07
FeO	15.58	14.86	14.26	17.48	15.29	15.95	13.78	13.41	13.95	13.21	12.95	14.18	16.42	15.64	15.14
MgO	14.04	14.81	15.24	13.06	13.97	14.34	15.66	16.06	15.47	16.16	16.17	15.44	12.89	14.5	12.92
CaO	10.80	10.84	10.99	10.75	10.58	10.67	10.71	10.74	10.81	11.57	11.52	11.29	10.94	11.65	10.97
MnO	0.74	0.77	0.81	0.74	0.32	0.71	1.09	1.10	1.06	0.61	0.66	0.66	0.30	0.25	0.30
Na_2O	1.19	0.96	0.74	1.03	1.61	0.93	1.27	1.13	1.19	0.91	1.04	1.40	1.71	0.68	1.82
K_2O	0.44	0.39	0.29	0.46	0.47	0.37	0.34	0.34	0.39	0.25	0.32	0.50	0.59	0.19	0.63
Total	98.41	98.00	98.35	97.90	98.20	98.03	98.22	98.65	98.28	98.87	98.35	98.67	98.99	98.36	98.43
O	23	23	23	23	23	23	23	23	23	23	23	23	23	23	23
Cation	15	15	15	15	15	15	15	15	15	15	15	15	15	15	15
Si	6.99	7.20	7.31	7.03	6.70	7.18	7.32	7.29	7.34	7.45	7.42	7.17	6.33	7.27	6.32
Al^{iv}	1.01	0.80	0.69	0.97	1.30	0.82	0.68	0.71	0.66	0.55	0.58	0.83	1.67	0.73	1.68
Al^{vi}	0.08	0.05	0.07	0.05	0.09	0.05	0.02	0.02	0.03	0	0	0	0.10	0.05	0.22
Ti	0.09	0.08	0.06	0.07	0.19	0.06	0.09	0.10	0.07	0.05	0.06	0.12	0.23	0.02	0.24
Fe^{+2}	1.18	1.23	1.12	1.44	1.09	1.28	1.37	1.39	1.35	1.30	1.33	1.44	1.05	1.19	1.08
Fe^{+3}	0.62	0.44	0.49	0.59	0.61	0.50	0.16	0.14	0.17	0.16	0.12	0.11	0.84	0.61	0.67
Mg	3.03	3.20	3.26	2.86	3.02	3.11	3.37	3.35	3.38	3.48	3.49	3.34	2.78	3.12	2.80
Mn	0.09	0.09	0.10	0.09	0.04	0.09	0.12	0.13	0.13	0	0	0	0.04	0.03	0.04
Ca	1.68	1.68	1.69	1.69	1.65	1.66	1.69	1.68	1.66	1.79	1.79	1.75	1.70	1.79	1.71
Na	0.15	0.10	0.12	0.09	0.16	0.09	0.03	0.03	0.05	0	0.01	0	0.16	0.10	0.15
K	0.08	0.07	0.05	0.09	0.09	0.07	0.07	0.07	0.06	0.05	0.06	0.09	0.11	0.03	0.12
Total	14.99	14.95	14.96	14.96	14.93	14.91	14.91	14.91	14.91	14.84	14.85	14.84	15.01	14.96	15.02
CaB	1.68	1.66	1.68	1.69	1.65	1.66	1.69	1.68	1.66	1.79	1.79	1.75	1.70	1.79	1.71
NaB	0.15	0.14	0.10	0.09	0.16	0.09	0.03	0.03	0.05	0	0.01	0	0.16	0.10	0.15
NaA	0.19	0.14	0.17	0.20	0.30	0.17	0.29	0.30	0.31	0.25	0.29	0.40	0.32	0.09	0.36
KA	0.08	0.14	0.17	0.20	0.30	0.17	0.07	0.07	0.06	0.05	0.06	0.09	0.11	0.03	0.12
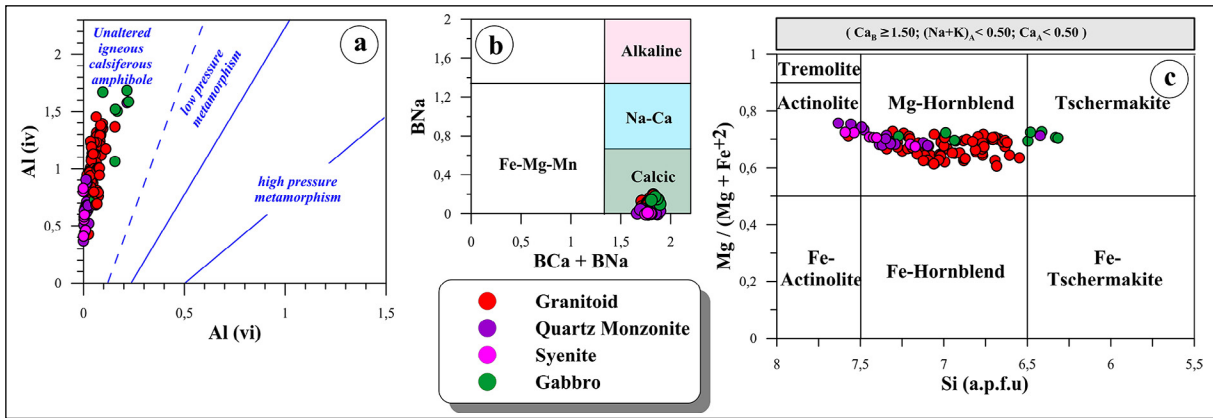
Figure 6- Amphiboles belong to the rock groups in the study area; a) Al^{iv} versus Al^{vi} change (Fleet and Barnett 1978), b) BNa versus BNa + BCa change and c) Species naming of crystals in the Mg/(Mg+Fe+2) versus Si diagram (Leake et al., 1997).

in the aforementioned diagram can be interpreted as the amphibole composition is concentrated in the Mg-hornblende area in samples belonging to rocks where the magma mixing/crust interaction is excessive. Accordingly, it is possible to say that mafic intrusions show homogeneous and less magma mixing effect, while felsic intrusions (granite, granodiorite, quartz monzonite and syenite) show more magma mixing effect.

As suggested by Ridolfi et al. (2010), pressure and temperature calculations were made in amphiboles. Accordingly, it was determined that it crystallizing of amphiboles in granites 0.56-1.19 kbar pressure, 745.25-799.62°C temperature; 0.37-1.28 kbar pressure, 704.07-872.33°C temperature in granodiorites; pressure of 0.42-0.56 kbar, temperature of 738.15-772.79°C in quartz monzonites; pressure range of 0.35-0.63 kbar, temperature range of 738.15-772.79°C in syenites; In the gabbros, the pressure range of 1.82-3.34 kbar and the temperature range of 862.15-919.61°C. Based on thid, it has been theoretically calculated that amphiboles in felsic intrusions crystallize between 3.61 km and 1.88 km on average, and amphiboles in mafic intrusions crystallize at an average depth of 9.97 km (Table 4). It is concluded that felsic intrusive rocks crystallize mostly in the upper crust and have a similar origin in that they come from similar depths. It has been shown that gabroic rocks derived from different sources may have crystallized at deeper depths (9.97 km) compared to granitoids by coming from deeper depths (lower crust-mantle). In addition, it is observed that both the

crystallization temperatures observed in felsic rocks and the excess of overlaps in the pressures of the medium in which they are formed may be due to the mixing of magma.

Table 4- Crystallization conditions and depths of intrusive rocks in the Strandja massif based on the chemical composition of minerals in amphiboles (Ridolfi et al., 2010).

Rock Types		Temperature (T) (C°)	Pressure (P) (kbar)	Depth (km)
Granite	*min*	745.25	0.56	2.16
	max	799.62	1.19	4.58
	ort	779.74	0.81	3.12
Granodio-rite	*min*	704.07	0.37	1.42
	max	872.33	1.28	4.93
	ort	814.49	0.94	3.61
Syenite	*min*	710.34	0.35	1.34
	max	797.49	0.63	2.42
	ort	761.57	0.51	1.96
Quartz Monzonite	*min*	738.15	0.42	1.61
	max	772.79	0.56	2.15
	ort	757.52	0.49	1.88
Gabbro	*min*	862.15	1.82	7.01
	max	919.61	3.34	12.86
	ort	892.82	2.59	9.97

5. Conclusion

Late Cretaceous aged subduction-related intrusions of in Strandja Massif have been studied in two groups as felsic and mafic intrusions. Felsic intrusions consist of granite, granodiorite, quartz monzonite and syenite, while mafic intrusions consist of diorite and gabbro. Markers of coeval magma mixing processes

are observed in Strandja intrusions with macroscopic and microscopic evidences. Mineral chemistry and Confocal Raman Spectrometry studies were carried out on amphibole crystals, which are common among all rock groups in the Strandja Intrusions, which are the product of magma mixing. According to the results of mineral chemistry of amphiboles, which are hydrous silicate minerals, calcic is Mg-hornblende type. According to P-T-d calculations made in amphibole crystals, felsic intrusions were crystallized under the pressure range of 0.35-1.28 kbar, 704.07-872.33°C temperature, at a depth of about 4.93 km to 1.34 km; mafic intrusions were crystallized at pressure of 1.82-3.34 kbar, at temperature of 862.15-919.61°C and at depth of 7.01-12.86 km. The fact that the felsic intrusions have similar and overlapping conditions both in the thermobarometric conditions of crystallization and in the depths where they crystallize at a higher rate of magma mixing, whereas the mafic intrusions exhibit different thermobarometric relationships and crystallize at different depths, which means that they originate from different sources and exhibit proportionally less magma mixing. In spectroscopic investigation performed with CRS, it was determined that felsic and mafic magma mixing was effective in the formation of amphiboles and that actinolite amphiboles crystallized more. As a result, amphibole minerals in the Strandja Intrusions, As a result, mineralogy, petrography, CRS and EPMA data of amphibole minerals in Strandja Intrusions point to similar petrological results, reflecting that felsic intrusions have similar origins and are formed as a result of magma mixing, whereas mafic intrusions are originated from deeper depth and are less affected by magma mixing.

Acknowledgement

References

Akçe, M. A., Kadıoğlu Y. K. 2020. Raman Spektroskopisinin İlkeleri ve Mineral Tanımlamalarında Kullanılması. Nevşehir Bilim ve Teknoloji Dergisi 9 (2), 99-115.

Apopei, A. I., Buzgar, N. 2010. The Raman study of amphiboles. Analele Stiintifice de Universitatii AI Cuza din lasi, Section 2. Geologie 56 (1), 57.

Aydın, Ü., Şen, P., Özmen, Ö., Şen, E. 2019. Petrological and geochemical features of Biga Peninsula granitoids, NW Anatolia, Turkey. Bulletin of the Mineral Research and Exploration 160 (160), 81-115.

Aydın, Y. 1974. Etude pétrographique et géochimique de la partie centrale du Massif d'Istranca (Turquie). Thsede Docteur, Universit de Nancy, 131, Ingnieur.

Aydın Y. 1982. Yıldız Dağları (Istranca) Masifi'nin jeolojisi. Doçentlik Tezi, İstanbul Teknik Üniversitesi, 106, İstanbul.

Aydın Y. 1988. Yıldız Dağları Masifi'nin Jeolojisi. Selçuk Üniversitesi Mühendislik Mimarlık Fakültesi Dergisi 2, 61-74.

Aydınçakır, E., Gündüz, R., Yücel, C. 2020. Emplacement conditions of magma (s) forming Jurassic plutonic rocks in Gümüşhane (Eastern Pontides, Turkey). Bulletin of the Mineral Research and Exploration 162 (162), 175-196.

Aykol, A. 1979. Kırklareli Demirköy Sokulumu'nun petroloji ve jeokimyası. Doktora Tezi, İTÜ, Maden Fakültesi, 204.

Aykol, A., Tokel, S. 1991. The geochemistry and tectonic setting of the Demirköy pluton of the Srednogorie–Istranca granitoid chain, NW Turkey. Mineralogical Magazine 55 (379), 249-256.

Bedi, Y., Ulusoy, E., Yusufoğlu H., Boncheva, I., Vasilev, E., Dabovski, C., Sachanski, V., Ivanova, D., Lakova, I. 2022. Istranca Kristalen Kompleksinin Tektonostratigrafik Özellikleri ve Bulgaristan'daki İstiflerle Korelasyonu Sonuç Raporu. Maden Tetkik ve Arama Genel Müdürlüğü, Ankara, 835.

Bodnar, R. J., Frezzotti, M. L. 2020. Microscale chemistry: Raman analysis of fluid and melt inclusions. Elements: an International Magazine of Mineralogy, Geochemistry, and Petrology 16 (2), 93-98.

Candan, O., Akal, C., Koralay, O. E., Okay, A. I., Oberhänsli, R., Prelević, D., Mertz-Kraus, R.

2016. Carboniferous granites on the northern margin of Gondwana, Anatolide-Tauride Block, Turkey–Evidence for southward subduction of Paleotethys. Tectonophysics 683, 349-366.

Catto, S., Cavazza, W., Zattin, M., Okay, A. I. 2018. No significant Alpine tectonic overprint on the Cimmerian Strandja Massif (SE Bulgaria and NW Turkey). International Geology Review, 60(4), 513-529.

Chatalov, G. 1988. Recent developments in the geology of the Strandzha Zone in Bulgaria. Bulletin Technical University of İstanbul, 41, 433-466.

Chukanov, N. V., Vigasina, M. F. 2020. Vibrational (Infrared and Raman) spectra of minerals and related compounds. Springer, Cham, Switzerland, 1-1376.

Çağlayan, M. A., Yurtsever, A. 1998. Burgaz-A3, Edirne-B2 ve B3; Burgaz-A4 ve Kırklareli-B4; Kırklareli-B5 ve B6; Kırklareli-C6 Paftaları, 1:100 000 ölçekli açınsama nitelikli Türkiye jeoloji Haritaları No: 20, 21, 22, 23. Maden Tetkik ve Arama Genel Müdürlüğü, Ankara.

Deniz, K. 2010. Buzlukdağı (Kırşehir) alkali magmatik kayaçların jeolojisi, petrolojisi ve konfokal raman spektrometresi ile incelenmesi. Yüksek Lisans Tezi, Ankara Üniversitesi Fen Bilimleri Enstitüsü Jeoloji Mühendisliği Ana Bilim Dalı, 138.

Deniz, K. 2022. Mica Types as Indication of Magma Nature, Central Anatolia, Turkey. Acta Geologica Sinica-English Edition, 96 (3), 844-857.

Deniz, K., Kadıoğlu, Y.K. 2019. Investigation of feldspar raw material potential of alkali feldspar granites and alkali feldspar syenites within Central Anatolia. Bulletin of the Mineral Research and Exploration 158 (158), 265-289.

Ferrando, S. 2018. Raman spectroscopy in Earth Sciences. GNM-SIMP "Physical Properties of Minerals" School, 12-15 February 2018, Brixen.

Ferraro J. R., Nakamoto, K., Brown, C. W. 2003. Introductory Raman Spectroscopy 2nd Ed. Academic Press. San Diego, 434.

Fleet, M. E., Barnett, R. L. 1978. Al iv/Al vi partitioning in calciferous amphiboles from the Frood Mine, Sudbury, Ontario. The Canadian Mineralogist 16 (4), 527-532.

Frezzotti, M. L., Tecce, F., Casagli, A. 2012. Raman spectroscopy for fluid inclusion analysis. Journal of Geochemical Exploration 112, 1-20.

Güllü, B., Kadıoğlu, Y. K., Koralay, T., Deniz, K. 2019. Raman characteristics of Gucunkaya (Aksaray)

gabbroic rocks, central Anatolia-Turkey. International Multidisciplinary Scientific GeoConference: SGEM, 28.06-07.07.2019, Albena, 475-482.

Kadıoğlu, Y. K., Deniz, K., Korala, T., Güllü, B. 2019. Nature of the gabbro in Central Anatolia: Geological observation and spectroscopic applications, Turkey. International Multidisciplinary Scientific GeoConference: SGEM, 28.06-07.07.2019, Albena, 377-384.

Karacan, M. S. 2020. "Enstrümental Analiz" Ders Notları, Ankara (unpublished).

Karacık, Z., Tüysüz, O., 2010. Petrogenesis of the Late Cretaceous Demirköy Igneous Complex in the NW Turkey Implications for the magma genesis in the Strandja Zone. Lithos, 114 (3-4), 369-384.

Kloprogge, J. T., Case, M. H., Frost, R. L. 2001. Raman microscopic study of the Li amphibole holmquistite, from the Martin Marietta Quarry, Bessemer City, NC, USA. Mineralogical Magazine 65 (6), 775-785.

Kuşçu, İ., Tosdal, R. M., Gençalioğlu-Kuşcu, G. 2019. Episodic porphyry (Cu-Mo-Au) formation and associated magmatic evolution in Turkish Tethyan collage. Ore Geology Reviews 107, 119-154.

Leake, B. E., Woolley, A. R., Arps, C. E., Birch, W. D., Gilbert, M. C., Grice, J. D., Hawthorne, F. C., Kato, A., Kısch, J. H., Krivovichev, G. V., Linthout, K., Laird, J., Mandarino, S. A., Maresch, V. W., Nickel, E. H., Schumacher, C. J., Smith, D. C., Stephenson, N. C. N., Ungaretti, L., Whittaker, E. J. W., Youzhi, G. 1997. Nomenclature of amphiboles; report of the subcommittee on amphiboles of the International Mineralogical Association, Commission on New Minerals and Mineral Names. Mineralogical Magazine, 61 (405), 295-310.

Makreski, P., Jovanovski, G., Gajović, A., Biljan, T., Angelovski, D., Jaćimović, R. 2006. Minerals from Macedonia. XVI. Vibrational spectra of some common appearing pyroxenes and pyroxenoids. Journal of Molecular Structure 788 (1-3), 102-114.

McMillan, P. F., Hofmeister, A. M. 2018. Infrared and Raman spectroscopy. In Spectroscopic Methods in Mineralogy and Geology, 99-160.

Moore, W. J., McKee, E. H., Akıncı, Ö. 1980. Chemistry and chronology of plutonic rocks in the Pontid mountains, northern Turkey. Inc Symposium European Copper Deposits congress 18-22

September, Belgrade, 209-216.

Nasdala, L., Schmidt, C. 2020. Applications of Raman spectroscopy in mineralogy and geochemistry. Elements: an International Magazine of Mineralogy, Geochemistry, and Petrology 16 (2), 99-104.

Natal'in B.A., Satir M., Sunal G., Toraman E. 2005. Structural and metamorfic evolution of the Stradja masif. Türkiye Bilimsel Teknik Araştırma Kurumu, Yer Deniz Atmosfer Bilimleri ve Çevre Araştırma Grubu, Ankara.

Natal'in, B. A., Sunal, G., Gün, E., Wang, B., Zhiqing, Y. 2016. Precambrian to Early Cretaceous rocks of the Strandja Massif (northwestern Turkey): evolution of a long lasting magmatic arc. Canadian Journal of Earth Sciences, 53 (11), 1312-1335.

Ohta, E., Doğan, R., Batık, H., Abe M. 1988. Geology and mineralization of Dereköy porphyry copper deposit, northern thrace, Turkey. Bulletin of the Geological Survey of Japan 39 (2), 115-134.

Okay, A. I., Bozkurt, E., Satır, M., Yiğitbaş, E., Crowley, Q. G., Shang, C. K. 2008. Defining the southern margin of Avalonia in the Pontides: Geochronological data from the Late Proterozoic and Ordovician granitoids from NW Turkey. Tectonophysics, 461 (1-4), 252-264.

Okay, A. I., Satır, M., Tüysüz, O., Akyüz, S., Chen, F. 2001. The tectonics of the Strandja Massif: Late-Variscan and mid-Mesozoic deformation and metamorphism in the northern Aegean. International Journal of Earth Sciences, 90 (2), 217-233.

Okay, A. I., Tüysüz, O. 1999. Tethyan sutures of northern Turkey. Durand, B., Jolivet, L., Horvath, F. Serrane, M. (Ed). The Mediterranean Basins Tertiary Extension within the Alpine Orogene. Geological Society of London, Special Publications 156, 475-515.

Okay A. I., Yurtsever, A. 2006. Trakya Bölgesi litostratigrafi birimleri: Stratigrafi komitesi litostratigrafi birimleri serisi-2. Maden Tetkik ve Arama Genel Müdürlüğü Yayınları, 1-41.

Özdamar, Ş., Roden, M. F., Zou, H., Billor, M. Z., Hames, W., Georgiev, S., Dunkl, I. 2021. Petrogenesis of oligocene plutonic rocks in western Anatolia (NW Turkey): Insights from mineral and rock chemistry, Sr-Nd isotopes, and U-Pb, Ar-Ar and (U-Th)/He geochronology. Geochemistry, 81 (2), 125747.

Petry, R., Mastalerz, R., Zahn, S., Mayerhöfer, T. G., Völksch, G., Viereck-Götte, L., Kreher-Hartmann, B., Holz, L., Lankers, M., Popp, J. 2006. Asbestos mineral analysis by UV Raman and energy-dispersive X-ray spectroscopy. Chemphyschem: a European Journal of Chemical Physics and Physical Chemistry, 7 (2), 414-420.

Raman, C. V., Krishnan, K.S., 1928. The Negative Absorption of Radiation. Nature 122 (3062), 12–13.

Ridolfi, F., Renzulli, A., Puerini, M. 2010. Stability and chemical equilibrium of amphibole in calc-alkaline magmas: an overview, new thermobarometric formulations and application to subduction- related volcanoes. Contributions to Mineralogy Petrology, 160 (1), 45-66.

Rinaudo, C., Belluso, E., Gastaldi, D. J. M. M. 2004. Assessment of the use of Raman spectroscopy for the determination of amphibole asbestos. Mineralogical Magazine, 68 (3), 455-465.

RRUFF (Database of Raman spectra, X-ray diffraction and chemistry data for minerals). http://rruff.info/. 27.02.2021

Skoog D. A., Holler F. J., Nieman T. A. 1998. Principles of Instrumental Analysis. Saunders College Publishing, 849.

Sunal, G., Natal'in, B.A., Satır, M., Toraman E. 2006. Paleozoic magmatic events in the Strandja Massif, in NW Turkey. Geodinamica Acta, 19 (5), 283- 300.

Şengör, A. C., Yılmaz, Y. 1981. Tethyan evolution of Turkey: a plate tectonic approach. Tectonophysics, *75* (3-4), 181-241.

Ulusoy, E. 2012. Demirköy (Kırklareli) intrüzif kayaçlarının jeolojisi ve petrolojisi. Yüksek Lisans Tezi, Ankara Üniversitesi Fen Bilimleri Enstitüsü Jeoloji Mühendisliği Ana Bilim Dalı, 135.

Ulusoy, E. 2021. Istranca Masifindeki Mesozoyik intrüziflerinin tektonomagmatik evrimi, KB Türkiye/Tectonomagmatic evolution of Mesozoic intrusives of Strandja Massif, NW Turkey. Doktora Tezi, Ankara Üniversitesi, Fen Bilimleri Enstitüsü, Jeoloji Mühendisliği Ana Bilim Dalı, 258.

Ulusoy, E., Kadıoğlu, Y. K. 2021. Petrography and geochemical decomposition parameters of crystalline rocks; Demirköy intrusive body (DIB), NW Turkey. Bulletin of the Mineral Research and Exploration 165 (165), 253-365.

Üşümezsoy, Ş. 1990. Istranca orojeni; Karadeniz çevresi Kimmerid orojen kuşakları ve masif sülfit yatakları. Türkiye Jeoloji Bülteni 33 (1), 17-28, Ankara.

Watenphul, A., Burgdorf, M., Schlüter, J., Horn, I., Malcherek, T., Mihailova, B. 2016. Exploring the potential of Raman spectroscopy for crystallochemical analyses of complex hydrous silicates: II. Tourmalines. American Mineralogist, 101 (4), 970-985.

Young, A. T. 1981. Rayleigh scattering. Applied Optics, 20 (4), 533–535.

Zoroğlu, O., Kadıoğlu, Y. K. 2007. Behavior of amphiboles in the determination of magma zoning using confocal Raman spectrometry: Beypazarı Oymaağaç granitoid-Ankara Turkey. In Second International Conference on Geo-Resources in The Middle East and North Africa (GRMENA-2), 24-28 February 2007, Egypt, 110-111.